

# Post-correlation beamformer for time-domain studies of pulsars and transients

Jayanta Roy<sup>1</sup>, Jayaram N. Chengalur<sup>1</sup>, Ue-Li Pen<sup>2345</sup>

## ABSTRACT

We present a detailed analysis of post-correlation beamforming (i.e. beamforming which involves only phased sums of the correlation of the voltages of different antennas in an array), and compare it with the traditionally used incoherent and phased beamforming techniques. Using data from the GMRT we show that post-correlation beamformation results in a many-folds increase in the signal-to-noise for periodic signals from pulsars and several order of magnitude reduction in the number of false triggers from single pulse events like fast radio bursts (FRBs). This difference arises primarily because the post-correlation beam contains less red-noise, as well as less radio frequency interference. The post-correlation beam can also be more easily calibrated than the incoherent or phased array beams. We also discuss two different modes of post-correlation beamformation, viz. (1) by subtracting the incoherent beam from the coherent beam and (2) by phased addition of the visibilities. The computational costs for both these beamformation techniques as well as their suitability for studies of pulsars and FRBs are discussed. Techniques discussed here would be of interest for all upcoming surveys with interferometric arrays. Finally, we describe a time-domain survey with the GMRT using the post-correlation beamformation as a case study. We find that post-correlation beamforming will improve the current GMRT time-domain survey sensitivity by  $\sim 2$  times for pulsars with periods of few 100s of millisecond and by many-folds for even slower pulsars, making it

---

<sup>1</sup>National Centre for Radio Astrophysics, Tata Institute of Fundamental Research, Pune 411 007, India

<sup>2</sup>Canadian Institute for Theoretical Astrophysics (CITA), 60 St. George Street, Toronto, Canada M5S 3H8

<sup>3</sup>Dunlap Institute for Astronomy and Astrophysics, University of Toronto, Toronto, ON M5S 3H4, Canada

<sup>4</sup>Canadian Institute for Advanced Research, CIFAR Program in Gravitation and Cosmology, Toronto, ON M5G 1Z8, Canada

<sup>5</sup>Perimeter Institute for Theoretical Physics, Waterloo, ON N2L 2Y5, Canada

one of the most sensitive surveys for pulsars and FRBs at low and mid radio frequencies.

## 1. Introduction

Despite over five decades of pulsar surveys there are only  $\sim 2600$  pulsars that have been discovered so far<sup>6</sup>. This is 5% or less of the total Galactic population of pulsars (estimates of the Galactic population range from 40,000 to 90,000 objects, see e.g. Lorimer (2008)) and a large population of pulsars remains to be discovered by current and future surveys. Even though there has been an accelerating rate of discovery over the last decade, this has not been uniform across the entire parameter space occupied by pulsars. For example, even though the population of known Galactic field millisecond pulsars (MSPs) has increased approximately 4 fold over the last decade<sup>7</sup>, there has only been a  $\sim 40\%$  increase in the number of known slow pulsars (i.e. pulsars with period,  $P > 30$  ms). This very modest increase in the number of known slow pulsars is particularly unfortunate, since the already known population of relatively slow pulsars contains several interesting objects, such as double neutron stars ( $\sim 15$  known, Tauris et al. (2017)), which enable tests of strong field gravity, energetic young pulsars with significant spin-down noise, normal pulsars showing intermittency, drifting, and nulling, probing hitherto unknown emission physics, magnetars with extraordinary high magnetic fields ( $\sim 29$  known<sup>8</sup>), ultra slow pulsars (only 2 known) with period  $> 10$ s which graze the theoretical death-line. One of the major reasons for the relatively slow increase in the number of such known pulsars is that the detection of these objects via periodicity searches can be severely affected by both instrumental red-noise and radio frequency interference (RFI). Both of these phenomena particularly reduce the search sensitivity at the low frequency end of the power spectrum of the detected time series, which is where the signal from these objects is strongest.

In addition to pulsars, the population of time-domain radio transients consists of Rotating Radio Transients (McLaughlin et al. (2006); 112 known<sup>9</sup>) and Fast Radio Bursts (Lorimer et al. (2007), Thornton et al. (2013); 33 known<sup>10</sup>). All the Fast Radio Bursts

---

<sup>6</sup><http://www.atnf.csiro.au/people/pulsar/psrcat/>

<sup>7</sup><http://astro.phys.wvu.edu/GalacticMSPs/GalacticMSPs.txt>

<sup>8</sup><http://www.physics.mcgill.ca/~pulsar/magnetar/main.html>

<sup>9</sup><http://astro.phys.wvu.edu/rratalog/>

<sup>10</sup><http://www.frbcat.org/>

(FRBs) discovered to date are single events (except for one repeating FRB) of millisecond duration with dispersion measure (DM) values generally higher than the possible Galactic contribution. The non-repeating nature of these sources warrants real-time time-domain detections aided by simultaneous millisecond time-scale imaging to localize these events in order to maximise the science returns. Rotating Radio Transients (RRATs) show occasional flashes of dispersed radio bursts of typically a few milliseconds duration. The cause of their sporadic emission as well as their connection to other neutron star populations are not fully understood. Detection of a large number of FRBs and RRATs is essential in order for us to gain a better understanding of the nature of these sources. However, detection of such single pulse events with millisecond duration in dedispersed time-series data is severely hindered by the presence of RFI.

Time-domain surveys are generally sensitivity limited, hence surveys with more sensitive instruments should lead to a higher discovery rate. Many of the existing as well as future high sensitivity radio telescopes are interferometric arrays. Planned surveys with telescopes like MeerKAT (e.g. TRAPUM<sup>11</sup>), SKA Phase1 (e.g. Levin et al. 2017) also need to optimally combine signals from many small telescopes (i.e. do “beamformation”). The GMRT was one of the first interferometric instruments to be systematically used for pulsar searches. The high discovery rate of the GMRT High Resolution Southern Sky (GHRSS<sup>12</sup>; Bhattacharyya et al. (2016); Bhattacharyya (2017)) as well as the Fermi-directed survey (Bhattacharyya et al. 2013) demonstrate the capabilities of the GMRT for low frequency pulsar searches. The recent upgrade of the GMRT allowing much larger instantaneous bandwidths (uGMRT; Gupta et al. (2017)) brings a significant increase in its theoretical survey sensitivity for pulsars and FRBs at low and mid radio frequencies. With the uGMRT, phase-2 of the GHRSS survey (Roy 2018) is expected to achieve a sensitivity better than all existing and ongoing off-galactic plane surveys. Most of the existing and planned surveys however use one of the two traditionally used methods of beamformation, viz. Incoherent Array (IA) or Phased Array (PA) beams, which are described in more detail below. In this paper we explore the possibility of significantly improving the observed time-domain sensitivity using yet another kind of beamformation, viz. “post-correlation beamforming”. We show that in this kind of beamforming, the contribution of instrumental red-noise to the power spectrum is significantly reduced, thus greatly improving the sensitivity towards low and mid spin frequency pulsars. We also show that post-correlation beamformation can be used to significantly reduce the effect of RFI, thus improving the time-domain sensitivity for periodicity and sin-

---

<sup>11</sup><http://www.trapum.org/>

<sup>12</sup><http://www.ncra.tifr.res.in/ncra/research/research-at-ncra-tifr/research-areas/pulsarSurveys/GHRSS>

gle pulse search. Both of these factors lead to reduction of the number of false detections by several orders of magnitude. This not only allows one to lower the candidate detection threshold (i.e. probe fainter flux levels) but also greatly eases the problem of carrying out on-the-fly imaging and other follow-up of these events to maximize the science returns.

## 2. Beamformation with Antenna Arrays

### 2.1. Incoherent Array and Phased Array beamformation

Two commonly used beamformation techniques for antenna arrays are Incoherent Array (IA) beamformation and Phased Array (PA) beamformation. For example, the GMRT backends (GSB; Roy et al. (2010) or GWB; Reddy et al. (2017)) allow one to form both these type of beams by making per spectral channel combinations of the delay and fringe corrected signals from different antennas. The Incoherent Array (IA) beam is formed by summing together the squares of the individual antenna voltages, i.e. it adds together the signal powers. Mathematically

$$P_{\text{IA}} = \sum_{i=0}^{N-1} |V_i|^2 \quad (1)$$

where  $P_{\text{IA}}$  is the IA beam signal and  $V_i$  are the voltages from the individual antennas. This kind of combination leads to a wide field-of-view (but at reduced sensitivity compared to a phased combination) and is useful for blind searches (such as, for e.g. the GHRSS survey). The coherent or Phased Array (PA) beam is produced by summing together the voltages (after phasing them appropriately so that the beam points to the direction of interest) and then squaring the resultant sum. Mathematically,

$$P_{\text{PA}} = \left| \sum_{i=0}^{N-1} V_i e^{-i\phi_i} \right|^2 \quad (2)$$

where  $P_{\text{PA}}$  is the PA beam signal and  $V_i$  are the delay and fringe corrected voltages from the individual antennas, and  $\phi_i$  is the phase introduced in antenna  $i$  in order to steer the beam towards the desired direction. The PA beam has higher sensitivity than the IA beam. The signal-to-noise ratio ( $S/N$ ) for observations of a single pulse of flux density  $S$  located at the pointing centre of a dual polarized array for the IA and PA beam are:

$$(S/N)_{\text{IA}} = \frac{GS\sqrt{2N_a\Delta\nu\tau}}{T_{\text{sys}}} \quad (3)$$

$$(S/N)_{PA} = \frac{GSN_a\sqrt{2\Delta\nu\tau}}{T_{\text{sys}}} \quad (4)$$

where  $G$  is the gain of a single telescope,  $N_a$  is the number of antennas used for beam-formation,  $\Delta\nu$  is the instantaneous observing bandwidth,  $\tau$  is the integration time and  $T_{\text{sys}}$  is the total system noise. These expressions assume that the sky noise is small compared to the receiver noise of the antennas. The sensitivities of the IA and PA beams under different scenarios are discussed in detail in Kudale and Chengalur (2017).

The IA beam is not only less sensitive than the PA beam, it is also more vulnerable to instrumental gain fluctuations and RFI. This is because the IA beam is the sum of the auto-correlations of the individual antennas. Since most of the terms in the PA beam correspond to cross-correlations between antennas, it has some immunity to RFI (which gets decorrelated by the delay tracking/fringe rotation operations) as well as to fluctuations in the instrumental gains. We illustrate this by showing in Fig. 1 the dedispersed time-series for PSR J2144–3933 from simultaneous IA and PA observations using the GMRT. As can be seen, fewer RFI bursts are seen in the PA beam as compared to the IA beam. The PA beam noise properties in general appear better than those of the IA beam; one can see individual single pulses in the de-dispersed *PRESTO* (Ransom et al. 2002) output, while these pulses are lost in the noise of the IA beam. Still further improvement in the noise properties can be seen in the post-correlation beam output (the lowest panel in the figure). We discuss this in more detail below.

## 2.2. Post-Correlation Beamformation

Post-correlation (PC) beamformation (e.g. Kudale and Chengalur (2017)), conceptually consists of forming the desired beam not by combining the individual antenna voltages, but rather by combining the (suitably phased) visibilities from the different baselines in the array. Effectively, this eliminates the auto-correlation terms from the PA beam. According to the radiometer equation (3 and 4), for an array with  $N_a$  elements, in situations where sky noise is negligible (i.e.  $T_{\text{sky}} \ll T_{\text{rec}}$ ), the IA beam sensitivity scales as  $\sqrt{N_a}$ , whereas PA beam sensitivity scales as  $N_a$ . Following equation-29 of Kudale and Chengalur (2017), post-correlation beam sensitivity scales as  $\sqrt{N_a(N_a - 1)}$ . For a telescope like the GMRT with  $N_a = 30$ , the theoretical degradation of the sensitivity for the post-correlation beam compared to the PA beam is  $< 2\%$ . The reduction in sensitivity arises from the non inclusion of the  $N_a$  auto-correlation terms. However, in practice, since the auto-correlation signals are the ones which are most affected by instrumental gain fluctuations and RFI, one could in

fact (as can be seen in Fig. 1) get a significant improvement in the signal to noise ratio when using PC beamformation instead of PA beamformation. In addition, the PC beam is also easier to calibrate. Basically, as far as calibration is concerned, since the PC beam consists only of visibility data, and assuming that visibilities are also computed in parallel (as is the case for the GMRT) the beam can be calibrated using exactly the same techniques as standard interferometric imaging calibration. This holds also for polarimetric calibration. Since both the IA and the PA beams contain auto-correlation terms, proper calibration of these beams involves calibration of the system temperature. We note that calibration of the post-correlation beam could be done in real time, in situations where the visibility data is also output. For example, Kudale and Chengalur (2017)) demonstrate for the GMRT that it is possible to apply in real time phases obtained via in-field self calibration to keep the PA beam phased.

Although the name implies that post-correlation beamformation has to be done after correlating the antenna voltages, the beam can in fact be operationally produced in two different ways; (1) by subtracting the IA beam from the PA beam; this effectively removes all the auto-correlation data that is contained in the PA beam, or (2) by a phased addition of the cross visibilities. Mathematically, we could do either of

$$P_{\text{PC}} = \left| \sum_{i=0}^N V_i e^{-i\phi_i} \right|^2 - \sum_{i=0}^N |V_i|^2 \quad (5)$$

when using the antenna voltages directly, or

$$P_{\text{PC}} = 2 \times \text{Re} \left[ \sum_{i=0}^{N-1} \sum_{j=i+1}^{N-1} V_{ij} e^{-i\phi_{ij}} \right] \quad (6)$$

when using the visibilities. Here  $P_{\text{PC}}$  is the post-correlation beam signal,  $V_i$  and  $\phi_i$  are delay and fringe corrected voltages and the beam steering phase of the  $i^{\text{th}}$  antenna,  $V_{ij}$  and  $\phi_{ij}$  are the raw visibility and beam steering phase for the baseline between the  $i^{\text{th}}$  and  $j^{\text{th}}$  antenna. We also show in Fig. 2, schematic block diagrams of these two ways of forming the post-correlation beams. In section 4 we compare the computational costs of these two forms of beamformation.

### 3. Comparison of different beamformation schemes

We use a number of data sets to compare these different beamformation schemes. The first set of data is based on *SIGPROC*<sup>13</sup> *filterbank* data from uGMRT GWB backend observations in the 300-500 MHz band of the the slow ( $P \sim 8.5$  seconds) pulsar PSR J2144–3933. Data from the IA and PA beams formed in real time using the GWB were recorded, and the PC beam was formed offline using the difference between the PA and IA beams as described above (eqn. 5). Simulated pulsar signals were injected into the IA and PA *filterbank* data files using the *inject\_pulsar* routine of *SIGPROC* pulsar package. A total of 12 data sets (each for IA, PA and PA–IA) were generated in this way, where the difference between the data sets is the period of the injected pulsar signal, this varies from 25 ms to 128 seconds. The original data also of course contains the signal for PSR 2144–3933, making for a total of 13 data sets from the uGMRT data. In addition we also used data from GMRT GSB backend observations at 607 MHz of PSR J2144–3933. The Nyquist sampled antenna voltages were recorded on disk, and all beamformation as well as correlation was done offline. These data sets allow us to compare the performance of the different beamforming schemes with the exact same input data. The GSB data set also allows us to compare the two different ways of post-correlation beamformation discussed above.

In Fig. 3 we show the low frequency end of the power spectra after de-dispersion for the three different beamforming modes using the uGMRT data. As can be seen, the power spectra for the PA and IA beams are essentially the same, since, as mentioned above, this part of the power spectrum is dominated by the instrumental red noise and the RFI that is contained in the auto-correlation spectra. Consistent with this, the PC beam, which does not contain auto-correlation data has significantly lower noise. This ‘de-reddening’ of the power spectrum should greatly ease the problem of detecting slow pulsars. Indeed, one can see that in the PC beam, the signal from the 8.5 seconds pulsar is detectable from the 1st harmonic onwards. For the IA or PA beam on the other hand, only harmonics beyond the  $\sim 60$ th harmonic are visible in the power spectrum. Fig. 4 shows the folded profiles of PSR J2144–3933 for these IA, PA and PC beam data. A systematic and significant improvement in the signal to noise ratio is clearly visible even to the eye as one goes from the IA beam to the PA beam and PC beam. The PC beam’s SNR is  $\sim 5 - 6$  times better than that of the PA beam. This clearly shows the dramatic improvement in the detectability of slow pulsars when the noise and systematics contained in the auto-correlation spectra is eliminated. We note that the beams were formed using all of the input data, i.e. there has been no effort at RFI mitigation. We discuss below specific advantages the PC beam offers as far as targeted

---

<sup>13</sup><https://github.com/SixByNine/sigproc/>

removal of RFI is concerned.

In Fig. 5 we show the ratio of the SNRs of the PC and PA beams as a function of the pulse period. This plot was generated using the data for the simulated pulsars as well as the data for PSR J2144–3933. In all cases the PC beam has a higher SNR than the PA beam. The PC beam SNR is about 10% better than that of the PA beam for a spin period of 25 ms; this difference reaches factors of 5–6 for spin periods of  $\sim 10$  seconds. Beyond spin periods of  $\sim 10$  seconds, the increase in the SNR is not as large, but it is still as much as a factor of  $\sim 3$  for spin periods as long as 100 seconds, (i.e. spin frequency  $\sim 0.01$  Hz). This is due to the fact that red noise in PC beam also goes up below 0.1 Hz, as can be seen in Fig. 3.

The two methods of post-correlation beamformation presented in Sec. 2.2 are mathematically equivalent. One might imagine then that all that distinguishes these two methods is their respective computational costs. We discuss this issue in Sec. 4 below. However, there is one further way in which these two methods are different, viz. in the possibilities that they offer for identifying and removing RFI. When the PC beam is formed as the PA–IA beam, one can only flag out data at the granularity of an antenna. When forming the PC beam from the visibilities, one can flag out data at the granularity of baselines. This is particularly useful in arrays which contain antennas at a range of separations. Often data from the short baselines contain significantly more RFI than the data from long baselines. Since nearby antennas also have baselines with more distant antennas, this could allow one to greatly eliminate the RFI while retaining much of the raw sensitivity. We show in Fig. 6 that short time-scale (i.e. few seconds) RFI bursts present in the PC (visibility based) beam can be removed by flagging out the data from all the baselines shorter than a  $\sim 450$  metres (i.e. 3% to 4% of the total GMRT baselines). As shown in the figure, these RFI burst generate pseudo pulse like features in the folded profile of PSR J2144–3933; flagging the short baseline very effectively mitigates the problem. We note that the flagging done here was “blind”, i.e. short baselines were flagged, without looking at the data quality on these baselines. In principle one could use flagging algorithms (for e.g. such as FLAGCAL Prasad and Chengalur (2012)) to automatically identify and flag only those baselines which actually do have RFI.

So far we have been comparing the characteristics of the IA, PA and PC beams as far as detecting pulsars are concerned. Another class of pulsed signals that is of great interest currently are transients such as FRBs which emit single pulses. While observing with an interferometric array, one can save the visibilities for candidate events, so that one could also image the field in order to localize any confirmed sources (see e.g. Bhat et al. (2013)). As discussed in detail in Bhat et al. (2013), in such searches, it is important to reduce false positives as much as possible, in order to minimize the amount of data that has to be saved



and processed. Since the PC beam contains far less RFI than the IA and PA beam, one would expect that the number of false positives in the PC beam would also be less than that for the other beamforming modes. Fig. 7 shows the number of candidates detected from IA, PA and PC beam for simulated FRB events with various DMs injected in the same uGMRT 300–500 MHz band data as discussed above. The signals were injected using the same *inject\_pulsar* routine, but with pulse period being much larger than the duration of the data (i.e. 60 seconds). The post-correlation beam is formed as PA–IA. There are 8 FRB events simulated at DM of 10, 20, 50, 100, 200, 500, 1000 and 2000  $\text{pc cm}^{-3}$ . *PRESTO* based single pulse search were performed for all these three beams over a range of DMs (indicated by the error-bars). As can be seen from the figure, the number of triggers from the PC beam is almost two orders of magnitude lower than that the IA beam even at a DM as high as 2000  $\text{pc cm}^{-3}$ . The number of false positives in the PC beam data is also a factor of  $\sim 5$  less than that found in the PA beam data. Interestingly, over the full FRB DM search space (i.e. 250 to 2600  $\text{pc cm}^{-3}$ ), the candidate detection rate is almost constant for the PC beam. The percentage of true positives at the highest (2000  $\text{pc cm}^{-3}$ ) DM value of the simulations for IA, PA and PC beams are 0.0004, 0.8 and 5 respectively. We note that this plot was generated for candidates detected above a threshold of  $5\sigma$  in order to make the uGMRT 300–500 MHz PC beam sensitive enough to detect all the known FRBs (ignoring frequency dependent scattering and spectral steepening). At this threshold the uGMRT IA beam detects only 30% of the known FRBs. Raising the threshold to  $10\sigma$ , generates only very few triggers from the PC beam for this data, whereas IA beam continues to be equally corrupted. The recently detected FRBs are all at the lower end of the FRB flux distribution, all of these will be completely missed at the sensitivity offered by the IA beam. As is the case for FRBs, the PC beam data would also contain far fewer false positives in searches for other transients such as RRATs (most of which have  $\text{DM} < 300 \text{ pc cm}^{-3}$ ). Both manual as well as automated searches for RRATs in the IA beam data would be swamped by the large number of false positives. Ways of overcoming this problem by forming multiple incoherent sub-array beams and using co-incidence filtering are discussed in Bhat et al. (2013). However splitting antennas in sub-arrays significantly reduces the survey sensitivity. Another major difference between the IA and PC beam is of course the field of view. In blind surveys one would like to have as large a field of view as possible, in which case PC beamformation is not competitive, unless one is able to form multiple beams. In the next section we detail the computational cost involved in forming multiple PC beams.

#### 4. Computational requirements

As discussed above, there are two different ways of forming the post-correlation (PC) beam. The first is via the difference of the PA and IA beams, while the second is via a phased addition of the visibilities. While the PC beamformed in these two ways is mathematically equivalent, we also saw that operationally the visibility route might have some advantage because of the better opportunities it provides for flagging data affected by RFI. Here we take a look at the difference in the amount of computation required to make the PC beam in these two ways. To start with, we note that correlators require a fan out of the data, i.e. in order to correlate the data from one antenna with all other antennas one needs multiple copies of the data stream. On the other hand beamformation operates on the data stream from each antenna independently, except in the final addition stage. This would lead to differences in architecture. Here we do not look at this in detail, but instead focus only on the number of computations required to make the PC beam in these two different ways.

We start by defining the parameters needed to determine the required computation, with the assumed value of the parameter for the GMRT (where relevant) given in parenthesis. Let the total number of beams to be formed (each with an independent phase center) be  $N_B$ . The total number of antennas is  $N_a$  (30), the bandwidth of operation  $B$  (200 MHz), the number of time samples in a given FFT block  $N_f$  (4096 for 2048 spectral channels) and the number of FFT blocks per integration  $N_b$ . In terms of these parameters the channel resolution is  $\Delta\nu = \frac{B}{N_f}$  and the integration time  $\Delta\tau = \frac{N_b N_f}{2B}$ .

The total computational load (in number of operations per second) for PA–IA beamformation for one integration is

$$5N_a N_b N_f \log N_f + N_B N_a N_b N_f + N_B N_f (N_a N_b + N_b - 1) + N_b N_a N_f + (N_a - 1)(N_b - 1)N_f + N_B N_f \quad (7)$$

and consists of the following components:

- $5N_a N_b N_f \log N_f$  for FFT
- $N_B N_a N_b N_f$  for fringe and fractional-delay corrections as well as beam steering
- $N_B N_f (N_a N_b + N_b - 1)$  for PA beamformation including addition, squaring and integration
- $N_b N_a N_f + (N_a - 1)(N_b - 1)N_f$  for IA beamformation including squaring, addition and integration
- $N_B N_f$  for the PA-IA operation

We note that for PA–IA beamformation the phase corrections for beam steering needs to be done before antenna addition, which requires working at the FFT resolution. However, since the maximum fringe rate of the GMRT is  $\pm 5$  Hz (Chengalur 1998), the maximum possible delay change even over a period as large as 1 ms is much smaller than the Nyquist sampling resolution. This means that for PC beam formation from the visibilities we can do the differential beam steering after the visibilities have been computed. The total computation load (in number of operations per second) for visibility based PC beamformation for one integration is

$$5N_a N_b N_f \log N_f + N_a N_b N_f + N_b N_f \frac{N_a(N_a - 1)}{2} + (N_b - 1) N_f \frac{N_a(N_a - 1)}{2} + N_B N_f \frac{N_a(N_a - 1)}{2} + N_B N_f \left[ \frac{N_a(N_a - 1)}{2} - 1 \right] \quad (8)$$

and consists of the following components:

- $5N_a N_b N_f \log N_f$  for FFT
- $N_a N_b N_f$  for fringe and fractional-delay corrections at the pointing centre (common to all beams)
- $N_b N_f \frac{N_a(N_a - 1)}{2} + (N_b - 1) N_f \frac{N_a(N_a - 1)}{2}$  for correlation including multiplications and additions
- $N_B N_f \frac{N_a(N_a - 1)}{2}$  for phase corrections required for steering the individual beams
- $N_B N_f \left[ \frac{N_a(N_a - 1)}{2} - 1 \right]$  for visibility addition for the beamformation

For the given GMRT configurations with 1600 beams, in PA–IA based PC beamformation (i.e. Eq 7), term 2 (fringe, fractional delay and beam steering) and 3 (PA) dominates equally and at least 20-times higher than any other terms. Whereas for visibility based PC beamformation (i.e. Eq. 8), term 4 (beam steering) and 5 (visibility addition) dominates, but they are only an order of magnitude higher than the next dominating term 2 (FFT). However the contributions of term 4 and 5 of Eq. 8 increase by many-folds than any other terms as beams are formed at high time resolution. Considering these, one would expect that PA–IA beamformation is computationally cheaper for a small number of high time resolution beams, while the visibility based beamformation would be computationally cheaper for a large number of beams at low time resolution. The cross over point would depend also on the total number of elements. We show in Fig. 8 a comparison of these two computational loads as a function of the total number of beams formed and the time resolution for a GMRT

like array of 30 antennas (upper panel) as well as an SKA Phase1 Mid like array of 256 antennas. For the GMRT array we use 200 MHz instantaneous bandwidth with 2048 spectral channels at  $163.84 \mu\text{s}$  (upper right) and 1.31 ms (upper left) time resolution. For SKA Phase1 Mid array (Levin et al. 2017) we use 300 MHz instantaneous bandwidth with 4096 spectral channels at  $64 \mu\text{s}$  (lower right) and 2.048 ms (lower left) time resolution. The figures clearly bring out the broad trends expected with time resolution and number of beams. For the GMRT, visibility beamformation is economical compared to PA–IA beamformation for time resolutions  $\geq 163.84 \mu\text{s}$  and for  $\geq 10$  beams. For SKA Phase1 Mid array, visibility beamformation is economical compared to PA–IA beamformation for time resolutions  $\geq 2.048 \text{ ms}$  and for  $\geq 800$  beams. A configuration with a small number of high-time resolution beams would be useful in searches for pulsars (specially MSPs) via targeted observations of globular clusters (GCs). GCs are the most likely hosts of exotic binary systems, like MSP-main sequence binaries, highly eccentric binaries, MSPs in evolutionary phases like Redback, Black Widow and MSP-Black Hole binaries, which may not form via normal stellar evolution in the disk. The multiple beams should be sufficient to cover the expected sky area within which MSPs expelled from the centre but which are still within the cluster tidal radius. A moderate number of high time-resolution beams offers an opportunity to greatly increase the pulsar timing efficiency in arrays where the individual elements have a large field of view, by allowing simultaneous observations of multiple pulsars (Stappers et al. 2018). A large number of lower time resolution beams (as would be cheaper via the visibility route) would be useful in blind searches for all but the fastest pulsars.

## 5. Case study of a proposed GMRT survey

The improvements seen in time-domain processing using post-correlation beamformation aided with the enhanced sensitivity of the uGMRT for the GHRSS phase-2 survey, provide the motivation to develop a time-domain survey with a post-correlation beamformer. We compute here the estimated parameters for such a survey. To benchmark, we consider the uGMRT 300–500 MHz band with 30 antennas, 200 MHz bandwidth, 2048 spectral channels, visibility beamformation at 1 ms time-resolution with about 128 beams covering  $\sim 10'$  FoV. We note that covering the entire field of view with PC beams would require  $\sim 1600$  beams. We estimate a survey sensitivity of  $\sim 0.1 \text{ mJy}$  at 400 MHz (considering the radiometer equation 4 with a 2% loss for ignoring the auto-correlation power), for a  $10\sigma$  detection for a 10% duty cycle, a post-correlation beam gain of 7 K/Jy for 200 MHz bandwidth, 10 mins of dwell time, and a system temperature of 106 K. We also calculate a sensitivity of 0.05 Jy as the  $5\sigma$  detection limit for 5 ms transient millisecond bursts, which would correspond to weak scattering (Thornton et al. 2013).

Fig. 9 shows the components required for such time-domain survey with the post-correlation beamformer as specified above. The required components are shown in four different colours. Visibilities computed in the uGMRT backend (GWB; marked in blue) at 1 ms time resolution are transferred to the the post-correlation beamformer nodes (marked in orange) with an aggregate data rate of  $\sim 3$  GB/s. We aim to implement in-field phasing (Kudale and Chengalur (2017)) using a sky model derived from the time-averaged visibilities in order to improve the coherence in phasing up to baseline length of several kilometers. This optimises the GMRT phased array sensitivity beyond central compact core (most current phased array observations use only the antennas in the central square). In addition of deriving the phasing model, a baseline based flag masking the bad baselines will also be generated in real-time from these time-averaged visibilities. Coherent additions of these visibilities will result in 128 of such visibility beams. The multi-DM search for single pulses (colored in yellow) on each of these visibility beams would need to be executed on a separate FRB cluster followed by coincidence filtering to remove spurious events (Bhat et al. 2013). It is also proposed to record these 128 beams with 1 ms time-resolution giving a total data rate of 200 MB/s into disk for quasi-realtime search for pulsars using the same cluster. We note that the proposed 1 ms time-resolution is sufficient to detect double neutron star systems, young pulsars, normal pulsars as well as object like radio magnetars. Visibility buffers corresponding to candidate single pulse events will be recorded at 1 ms time resolution covering the full DM sweep time-range. For a event at a DM of  $2000 \text{ pc cm}^{-3}$ , the total DM sweep time over 200 MHz band in uGMRT 300–500 MHz band is  $\sim 50$  seconds, which results in 40 GB buffer size on each of the post-correlation beam nodes. This means one can easily hold few buffers for accommodating the pipeline delay and flush them to a storage based on the real-time triggers. These visibilities will be processed through the processing blocks (marked in green) for millisecond imaging localization at quasi real-time. This block includes removal of dispersion delay followed by a flagging and calibration pipeline and snapshot imaging. We note that part of this imaging pipeline to localise time-domain events has already been demonstrated for the GHRSS phase-1 survey (Bhattacharyya et al. 2016).

## 6. Summary

In this paper, we demonstrate that use of post-correlation beamformer for radio interferometric array results in a many-fold increase of the detection significance of time domain events compared to the conventional incoherent and coherent array beamformer. This increase in sensitivity is driven by the lower red-noise and RFI contamination of the post-correlation beam. Post-correlation beamformation also allows one to use standard interferometric calibration techniques for calibrating the beam. We compare two different modes of

post-correlation beamformation, viz. (1) PA-IA beamformation, which does not require computation of the visibilities and (2) visibility beamformation where the beam is formed from the computed visibilities. We also show that the PA-IA beamformation is computationally economical for a small number of high time resolution beams. At low time resolutions, the visibility based beamformation is computationally cheaper. Visibility based beamformation also allows for better control in flagging/suppressing RFI. For multi-element feed system (e.g. Parkes multibeam system) or for phased array feed, the PC beam can also be used to subtract RFIs (correlated within the feed elements) from feed element response (Kocz et al. 2010). These new beamforming techniques could significantly improve the sensitivity of time-domain studies with both existing (e.g. uGMRT, JVLA) and upcoming (e.g. CHIME, Amiri et al. (2018); OWFA, Subrahmanya et al. (2017)) radio interferometric arrays. As a specific example, we have presented a proposed time-domain survey with the uGMRT.

## 7. Acknowledgments

We thank the computer group at GMRT and NCRA. We thank Mr. Harshavardhan Reddy of GMRT for insightful discussions on the data-rate issues in the GWB. We thank Mr. Sanjay Kudale of GMRT for trying out in-field phasing in generating post-correlation beams. Ue-Li Pen acknowledges NSERC for support. We also acknowledge the support of telescope operators during our test observations which also involves data intensive baseband recording observations. The GMRT is run by the National Centre for Radio Astrophysics of the Tata Institute of Fundamental Research.

## REFERENCES

- Amiri, M., Bandura, K., Berger, P., et al. 2018, submitted to ApJ, arXiv:1803.11235
- Bhat, N. D. R., Chengalur, J. N., Cox, P. J., et al., 2013, ApJS, 206, 2
- Bhattacharyya, B.; Roy, J.; Ray, P. S., et al., 2013, ApJ Letters, 773, 12
- Bhattacharyya, B.; Cooper, S.; Malenta, M., et al., 2016, ApJ, 817, 130
- Bhattacharyya, B., 2017, Proceedings of IAU Symposium 337 - Pulsar Astrophysics: The Next Fifty Years, arXiv:1712.04518.
- Chengalur, J. N., 1998, *Delay Tracking and Fringe Stopping for the GMRT Correlator*, NCRA technical report, available : <http://www.ncra.tifr.res.in/library/>.

- Gupta, Y., et al., 2017, *Current Science*, 113, 4.
- Kocz, J., Briggs, F. H., & Reynolds, J., *AJ*, 2010, 140, 2086.
- Kudale, S. & Chengalur, J. N., 2017, *Experimental Astronomy*, 44, 97.
- Levin, L., Armour, W., Baffa, C., 2017, *Proceedings of IAU Symposium 337 - Pulsar Astrophysics: The Next Fifty Years*, arXiv:1712.01008.
- Lorimer D. R., 2008, *LRR*, 11, 8 (arXiv:0811.0762).
- Lorimer, D. R., Bailes, M., McLaughlin, M. A., Narkevic, D. J., Crawford, F., 2007, *Science*, 318, 777.
- Lorimer, D. R. & Kramer, M., 2004, *Handbook of Pulsar Astronomy*, Vol. 4. Cambridge, UK, 211.
- McLaughlin M.A., Lyne A.G., Lorimer D. R., et al. 2006, *Nature*, 439, 817.
- Prasad, J., Chengalur, J. N. 2012, *Experimental Astronomy*, 33, 157.
- Ransom, S. M., Eikenberry, S. S., & Middleditch, J. 2002, *AJ*, 124, 1788.
- Reddy, S. H., et al., 2017, *JAI*, 6, 1641011-336.
- Roy J., Gupta Y., Ue-Li Pen, Peterson J.B., Kudale S., Kodilkar J., 2010, *Experimental Astronomy*, 28, 55.
- Roy J., 2018, *Proceedings of IAU Symposium 337 - Pulsar Astrophysics: The Next Fifty Years*, arXiv:1801.02826.
- Roy J., 2013, PhD Thesis, submitted to National Centre for Radio Astrophysics, Tata Institute of Fundamental Research, Pune, India.
- Roy J., Ray P. S., Bhattacharyya B. et al., 2015, *ApJL*, 800, 12.
- Stappers B. W., Keane E. F., Kramer M., Possenti A., Stairs I. H., 2018, *Phil. Trans. R. Soc. A* 376: 20170293.
- Subrahmanya, C. R., Manoharan, P. K., & Chengalur, J. N., 2017, *JApA*, 38, 10S.
- Thornton, D., Stappers, B., Bailes, M., et al., 2013, *Science*, 341, 53.
- Tauris, T. M., Kramer, M., Freire, P. C. C., et al., 2017, *ApJ*, 846, 170.

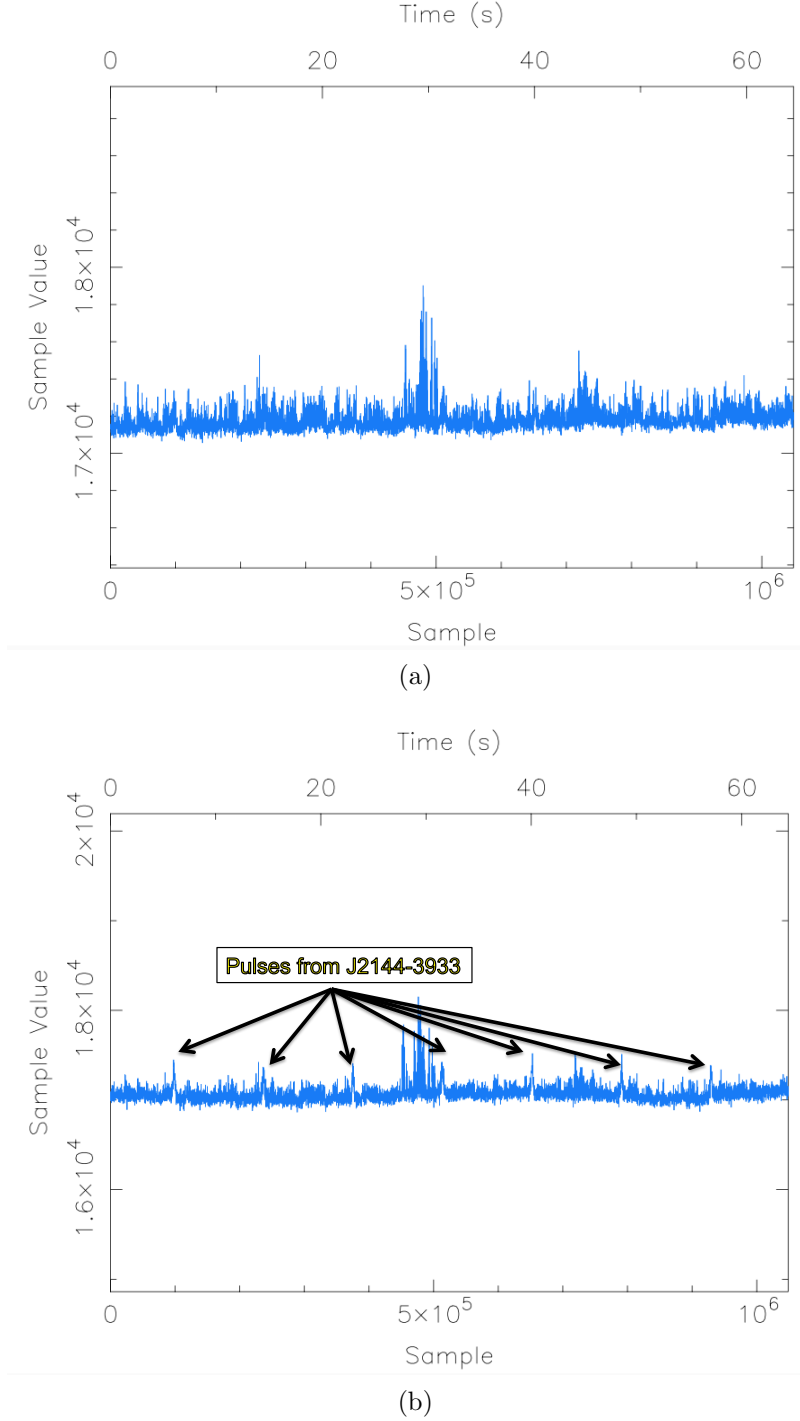


Fig. 1.— Dedispersed time-series for PSR J2144–3933 from simultaneous observations of (a) IA beam, (b) PA beam are shown here. The plots were generated using the *PRESTO* software tools. The plot shows the mean value computed using moving average of 8 time samples. The y-axis scale is different for the different panels. Fewer RFI bursts are seen in the PA beam as compared to the IA beam. Also individual single pulses (as marked in the plot) are visible for PA beam while these pulses are lost in the noise of the IA beam.



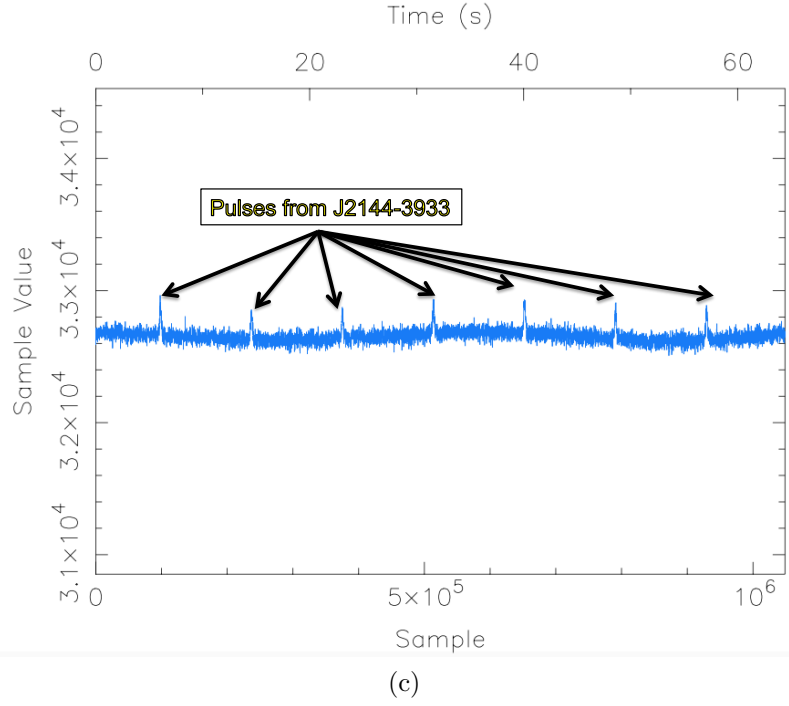


Fig. 1.— (c) Dedispersed time-series for PSR J2144–3933 from the post-correlation beam. As can be seen, there is a significant improvement in the immunity against RFI, and the individual pulses can be clearly seen.

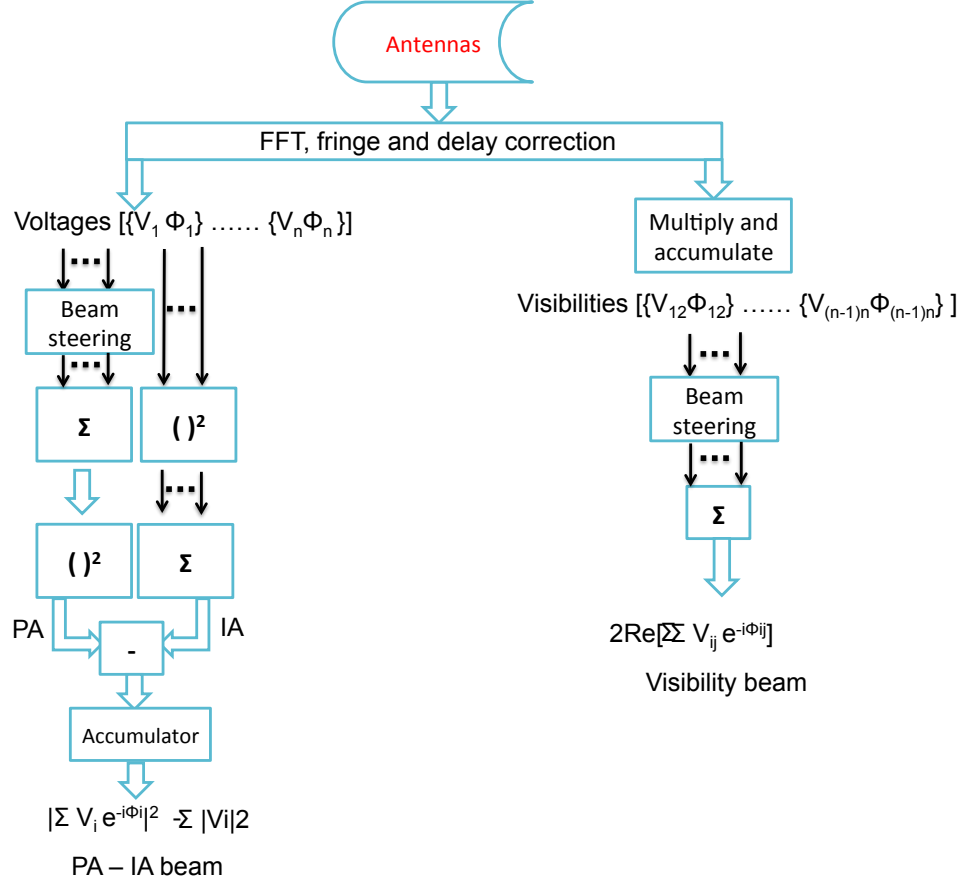


Fig. 2.— The schematic block diagram for post-correlation beamformation. The left branch shows PA-IA beamformation and the right branch shows beamformation using visibilities. Note that in PA-IA beamformation the beam steering has to be done at the FFT block level, while in visibility based beamformation the beam steering is done after accumulation.

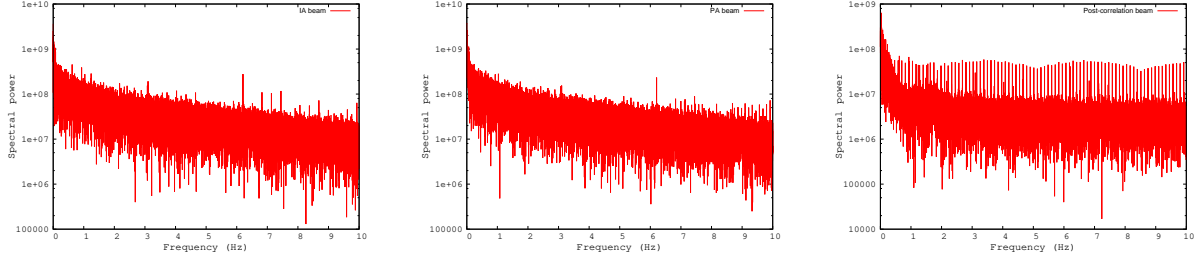


Fig. 3.— Power spectra for the IA, PA and PC beams for PSR J2144–3933. The harmonics of the pulsar are spaced at 0.12 Hz. As can be seen, the power spectra for the PA and IA beams are essentially the same. However, there is an order of magnitude reduction in red noise for the PC beam. This enables the detection of low order harmonics which are completely buried in the noise for the IA and PA beams. See the text for more details

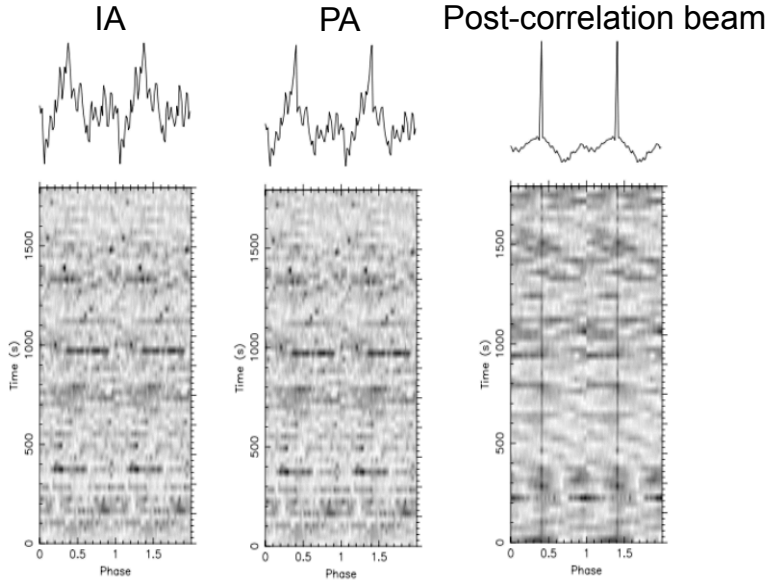


Fig. 4.— Folded profiles of PSR J2144–3933 observed with the uGMRT 300–500 MHz bands.

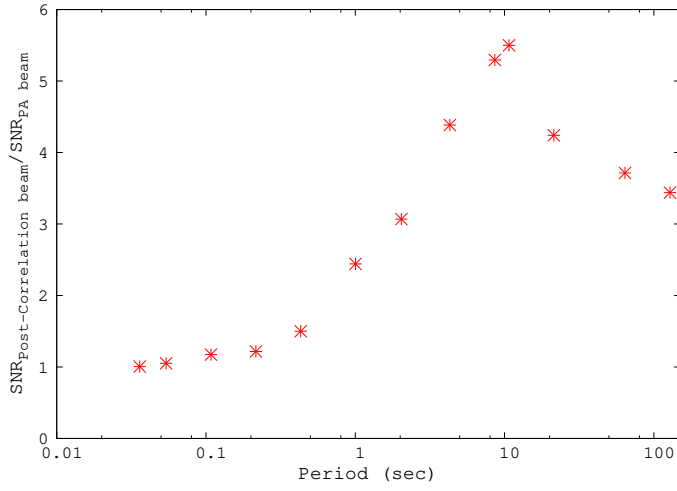


Fig. 5.— Sensitivity improvement with post-correlation beam compared to the PA beam as function of pulse period.

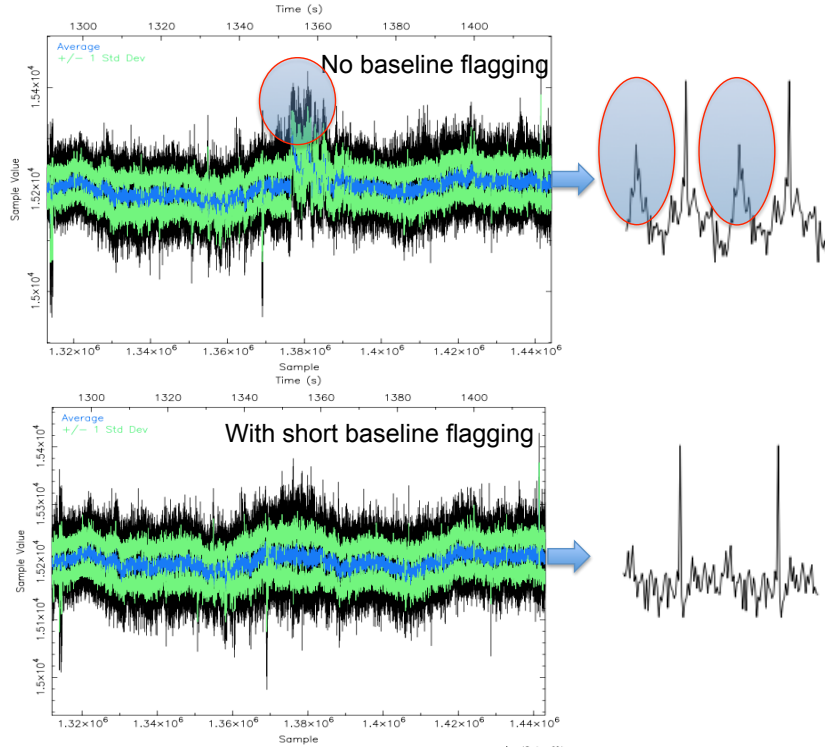


Fig. 6.— Visibility based post-correlation beamformation. The upper panel shows the time series when one uses all the data, while the lower panel shows the time series when the short baselines (which tend to be those most affected by RFI) are flagged. The plots on the side show the corresponding folded profiles. A dramatic decrease in the systematics can be seen when one flags the baselines with RFI. See the text for more details.

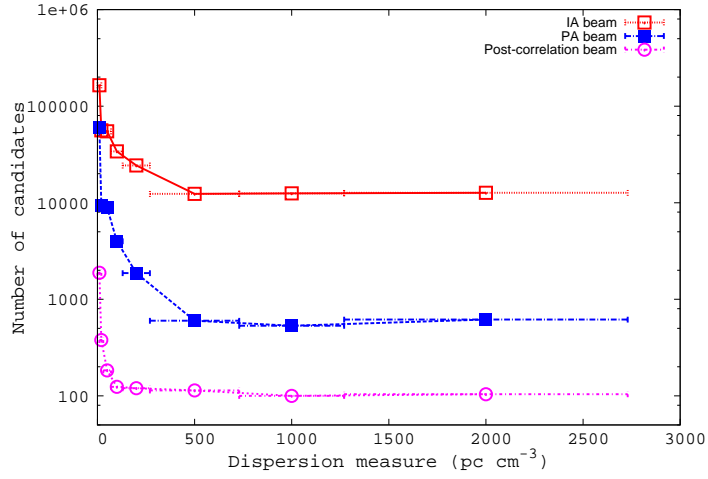
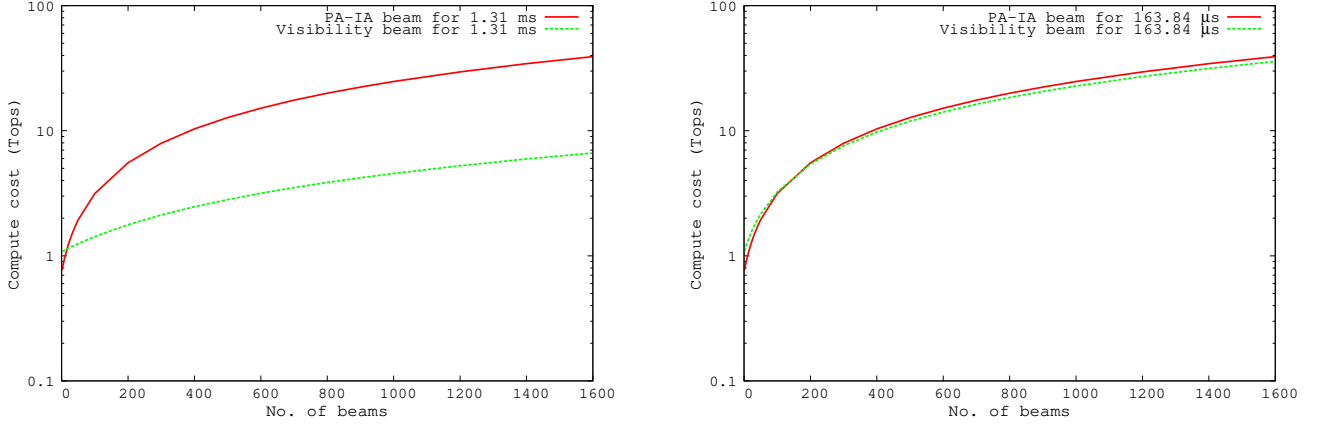
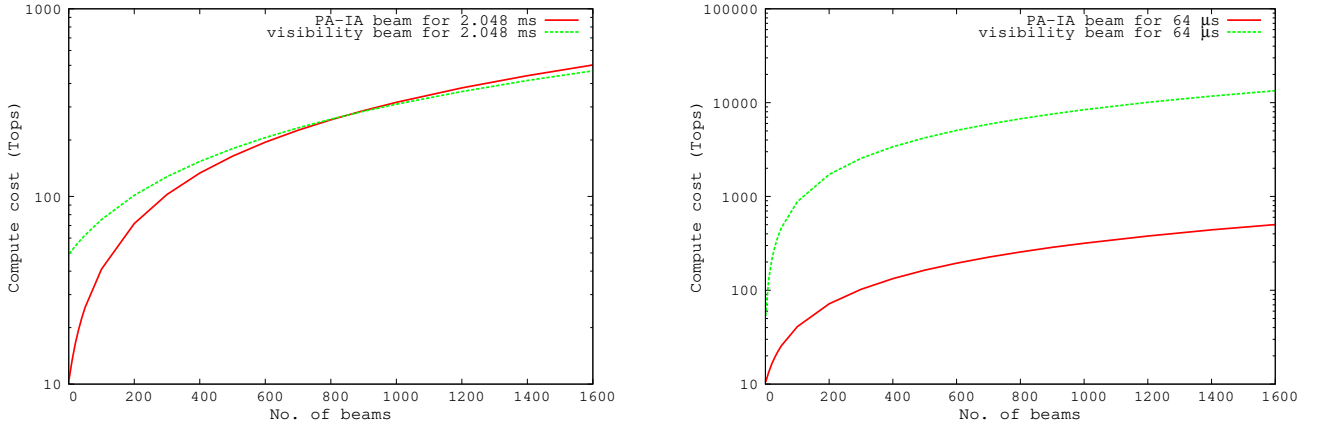


Fig. 7.— Number of candidate detected from IA, PA and post-correlation beam for simulated FRB events with various DMs for a data of 60 seconds duration. There are 8 FRB events simulated at DM of 10, 20, 50, 100, 200, 500, 1000 and 2000  $\text{pc cm}^{-3}$ . The DM range used in each steps for searches are shown by horizontal bars around each central DMs. This detection rate is for a threshold of  $5\sigma$ . The number of (false) detections from the IA beam is almost two order of magnitude higher than the post-correlation beam even at a DM of 2000  $\text{pc cm}^{-3}$ .



(a)



(b)

Fig. 8.— Comparison of compute costs for two ways of forming post-correlation beams for the GMRT (a) and the SKA Phase1 Mid array (b). For the GMRT, 1.31 ms (left panel) and 163.84  $\mu$ s (right panel) output time-resolution and for SKA Phase1 Mid, 2 ms (left panel) and 64  $\mu$ s (right panel) out time-resolution are plotted. PA-IA beams are marked in red and visibility beams are marked in green. Cost for both the beamformation modes are similar at 163.84  $\mu$ s time-resolution for GMRT and at 2 ms time-resolution for SKA Phase1 Mid.

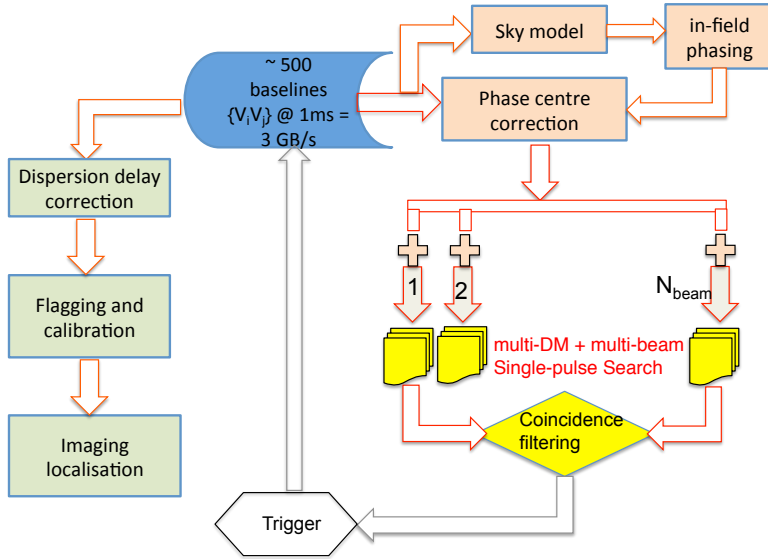


Fig. 9.— Proposed multi-beam time-domain survey with visibility beamformation. There are 4 functional modules each colored differently running on different compute hardware. Please refer to the text for further details.